

# Building World Class Microlithographic Lens Systems: Optical Material Requirements and Qualification Methods

Paul DeStefano and Paul Michaloski

Tropel  
60 O'Connor Road  
Fairport, NY 14450

## ABSTRACT

Building successive generations of state-of-the-art wide field, sub-micron microlithographic lens systems dictates ever-tightening material tolerances that challenge glass manufacturers. This paper discusses the optical material needs for microlithographic lens systems and Tropel's in-house material qualification program. Material qualification is divided into three successive stages: 1) fluorescence testing to qualitatively analyze color center characteristics of the material; 2) homogeneity testing to determine the relative volumetric variations in index; and 3) absolute index testing at multiple wavelengths to determine the material's dispersion characteristics.

## 1.0 INTRODUCTION

The material qualification system at Tropel can be divided into three areas: fluorescence testing, refractive index testing, and homogeneity testing. Fluorescence testing, as described below, provides information on the transmission of the material and absorption properties. Higher transmission in a material will obviously provide greater throughput. Heating effects, caused by absorption of energy by the material, will result in aberrations in the lens system due to changing physical properties of the material. Testing the index of refraction of the material, described elsewhere in this paper, provides the index of refraction at ultraviolet (UV) wavelengths which was not available from glass manufacturers when this testing was instituted. Also, this testing provides information at many wavelengths around the wavelength of interest so that a dispersion curve can be created. The dispersion information of the material is used to color correct the lens. Color correction errors in the lens are corrected by changing element curvatures. The absolute index measurement is needed for determining proper spacings between elements in the lens system. The homogeneity of the material is measured and compared to pass/fail criteria. Index inhomogeneities degrade lens performance even if very accurate surface figures are generated. All of the information mentioned above is necessary to build state-of-the-art microlithographic lens systems. This paper will discuss each process in the material qualification.

## 2.0 FLUORESCENCE TESTING

Fluorescence testing provides a quick method of qualifying material for absorption characteristics. Energy absorption by the material will limit the energy through-put and may result in damage to the material over time. Fluorescence testing involves irradiating a material with particle radiation,  $\gamma$ -rays, x-rays, or excimer laser radiation. Exposure to these types of radiation can cause

damage, or color centers, in silica. A color center is defined as a molecular structure change in the glass due to irradiation.<sup>1,2</sup>

## 2.1 Color centers

Three silica defects induced by these types of radiation include the E' center, the Non-Bridging Oxygen Hole Center [NBOHC], and the Peroxy Radical (O<sub>2</sub><sup>-</sup>).<sup>3</sup> The E' center is caused by radiation forming an e<sup>-</sup>-hole pair (exciton) which releases its energy through visible light or vibrations in the lattice. A large amount of vibrations concentrated in one area can break bonds which may then recombine and trap a free charge.<sup>4</sup> The NBOHC results when a silicon-oxygen bond breaks leaving a dangling, or non-bridging, oxygen atom and the generation of a free hydrogen atom. The Peroxy Radical (O<sub>2</sub><sup>-</sup>) is a combination of an oxygen molecule with an E' defect.<sup>3</sup>

The NBOHC defect causes an absorption of 257 nm radiation and a 'red' fluorescence in silica which is most noticeable in low OH<sup>-</sup>, or 'dry', silica. High OH<sup>-</sup>, or 'wet', silica is much less likely to exhibit the NBOHC defect and is the best choice for 248 nm applications.<sup>1,2</sup>

## 2.2 Testing process

Fluorescence testing at Tropel is accomplished by placing the sample in the beam of a 248 nm excimer laser and observing the color of the fluorescence. Since there are tight tolerances on the homogeneity, or amount of impurities, in the silica glass, most samples have similar fluorescence characteristics and usually fluoresce clear, very light green, light green, green, bright green, or very bright green. Samples that fluoresce 'red' have too much absorption near 248 nm and are not used for DUV applications. Thus, fluorescence testing provides a quick, simple test to spot potential absorption problems in silica.

## 2.3 Results

Comparing the results from fluorescence testing with those from index testing, an interesting correlation was found. The brighter green the fluorescence, the greater the index of refraction as seen in Fig. 2.1. Also, silica that appeared to have very little fluorescence was closer to Malitson's empirically derived value of index of refraction for fused silica.

## 3.0 HOMOGENEITY TESTING

The wavefront quality of an optical element is dependent on both the surface figure and the index homogeneity of the material. So, even if care is taken to fabricate very accurate surfaces on the lens blank, if the material is inhomogeneous, the transmitted wavefront will still be aberrated.

The traditional industry standard for describing homogeneity is based on a variation in the index of refraction of the material where

$$\Delta n = \frac{OPD}{t} \quad (3.1)$$

In this case,  $\Delta n$  is the change in the index of refraction throughout the sample,  $OPD$  is the optical path-length difference, and  $t$  is the thickness of the material. The homogeneity  $\Delta n$  of the material is found by accurately measuring the  $OPD$  using a double pass Fizeau interferometer to look through

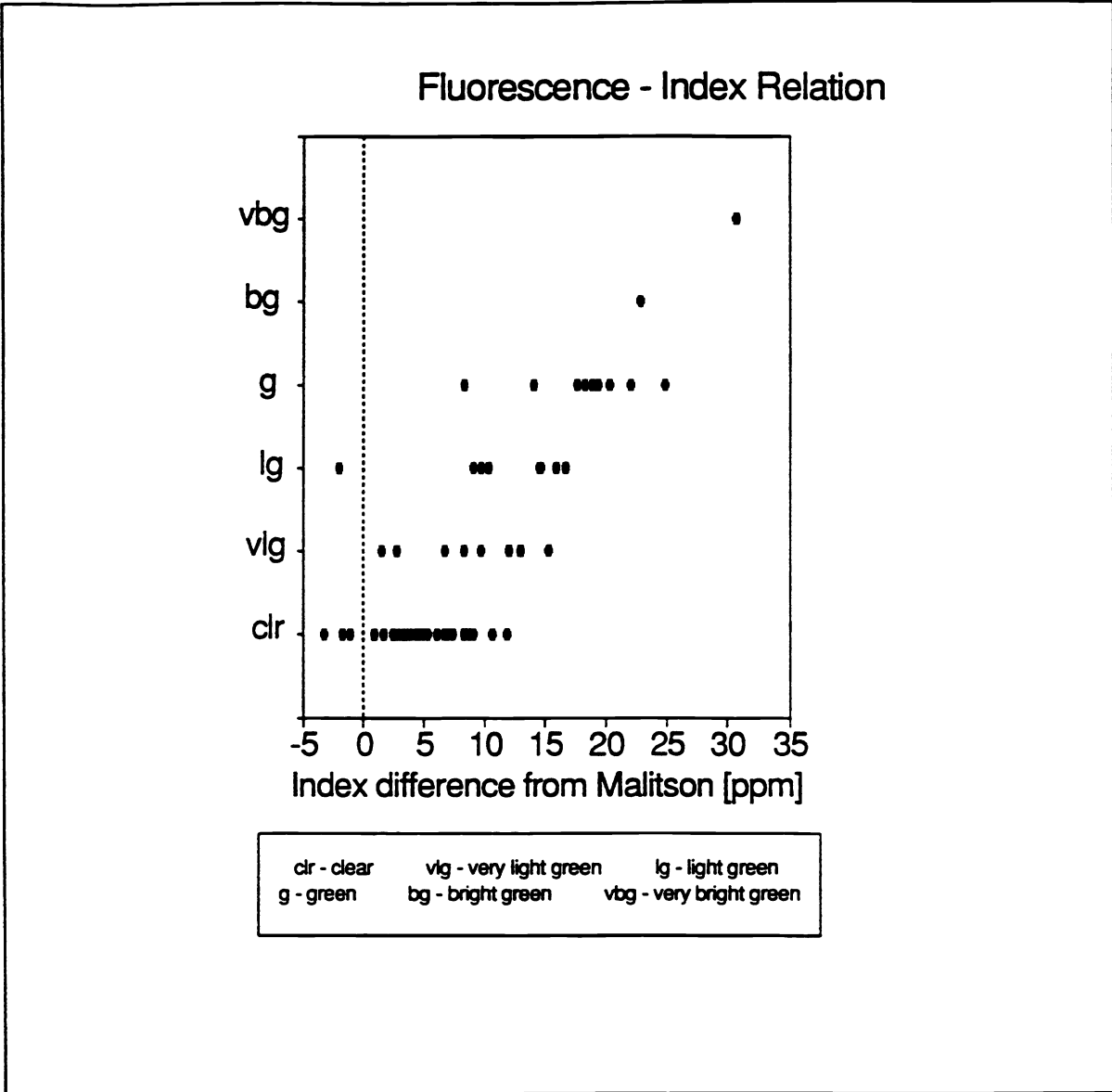


**Figure 2.1** Fluorescence test results in relation to index of refraction.

the material and then dividing the OPD by the thickness of the sample.<sup>5</sup> The material is then classified by group as:<sup>6</sup>

| <b><i>Homogeneity Group</i></b> | <b>H1</b>                              | <b>H2</b>                             | <b>H3</b>                             | <b>H4</b>                             |
|---------------------------------|----------------------------------------|---------------------------------------|---------------------------------------|---------------------------------------|
| <b><math>\Delta n</math></b>    | <b><math>\pm 20 \text{ E-6}</math></b> | <b><math>\pm 5 \text{ E-6}</math></b> | <b><math>\pm 2 \text{ E-6}</math></b> | <b><math>\pm 1 \text{ E-6}</math></b> |

The disadvantage of this grouping system is that it doesn't describe the character of the inhomogeneity. For example, a  $\pm 1 \text{ E-6 } \Delta n$  which occurs as a radial gradient may be tolerable in a design while a  $\pm 1 \text{ E-6 } \Delta n$  that occurs all at one edge of the lens blank may not. Thus, Tropel specifies

homogeneity in terms of Zernike polynomials to qualify glass for microlithographic and other precision lenses. Zernike polynomials are a set of orthogonal polynomials that can be used to describe a wavefront. The wavefront in this case relates to changes in the optical path-length deviations due to inhomogeneities in the material.

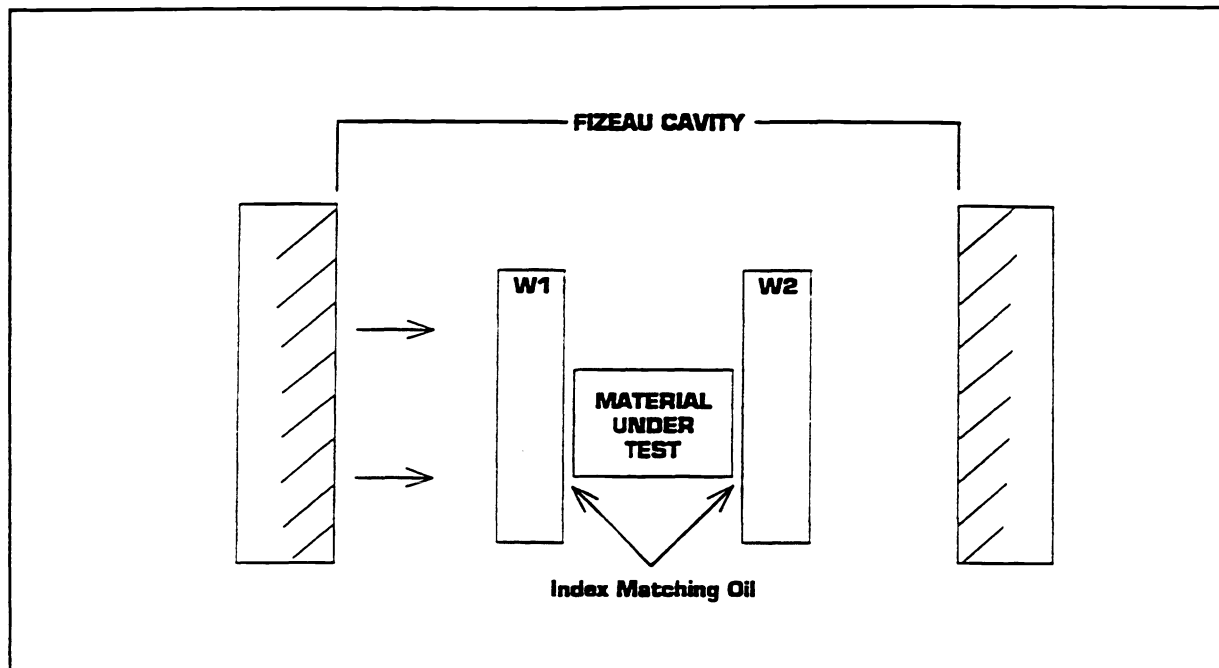


Figure 3.1 Traditional oil-on-window technique.

### 3.1 Traditional homogeneity testing

Traditionally, homogeneity testing is done by placing accurate windows on either side of a blank using index-matching fluid between the windows and the material under test [Fig. 3.1]. However, this process is messy, requires a long thermal stabilization period, and a poor registration of the windows can confound the test results. In order to combat these disadvantages, Tropel has developed a 'dunk test' in which the piece under test is immersed in index-matching oil [Fig. 3.2]. This instrument has an adjustable cavity length for different sized discs and allows for a faster stabilization period, more repeatable measurements, and more suited to high volume production.

Another process that can be used to measure homogeneity does not incorporate the use of index-matching fluids. This has the advantage of not requiring the handling of index fluids and cleaning solvents. However, it does require flats to be polished on the pieces instead of just rough ground surfaces. In addition, four tests must be run to collect data as opposed to one. These additional steps impede through-put and involve costly additions in the manufacturing process. Although theoretically the system errors subtract out, poor reproducibility was found when trying this technique. Thus, this test is not capable of testing index variations of less than  $5 \text{ E-}6$ .<sup>7,8</sup>

### 3.2 Tropel 'dunk' testing

To measure the OPD in the Tropel 'dunk tester', the setup in Fig. 3.2 is used. Any variations in the resulting wavefront are due to inhomogeneities of the material since the optical cavity is

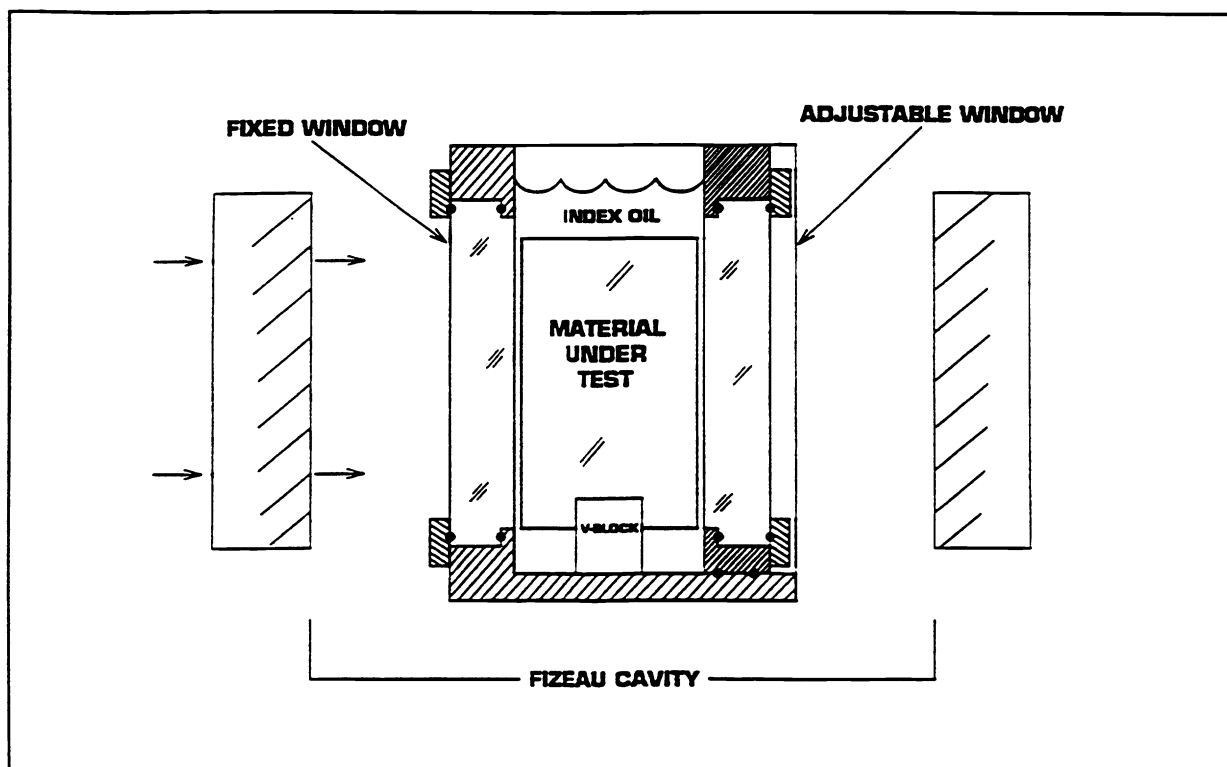


**Figure 3.2** Tropel homogeneity vessel, side view.

referenced first with no test piece in place. The sample test shown in Fig. 3.3 has a  $\Delta n$  well within the H4 homogeneity group; however, this part did not meet Tropel's Zernike specification due to the edge roll off.

#### 4.0 INDEX OF REFRACTION TESTING

Index of refraction testing was instituted due to a lack of available index data at UV wavelengths. The needed accuracy of the measurement required Tropel to develop a highly accurate index measurement tool.

##### 4.1 Why a prism refractometer?

A prism refractometer has been found to have distinct advantages over a number of different index measurement schemes. The proven technique has demonstrated the ability to yield accurate measurements from spectral lamps of low coherence compared to lasers. Spectral lamps have the advantages of low cost, low maintenance and many wavelengths for producing a more accurate fit to a dispersion equation. Another advantage is that the prism refractometer can read several wavelengths simultaneously, increasing the accuracy of the dispersion measurements and reducing the measurement time per sample. Lastly, prism refractometry, after a rigorous error analysis, has been shown that it is capable of producing measurements to the needed accuracy.

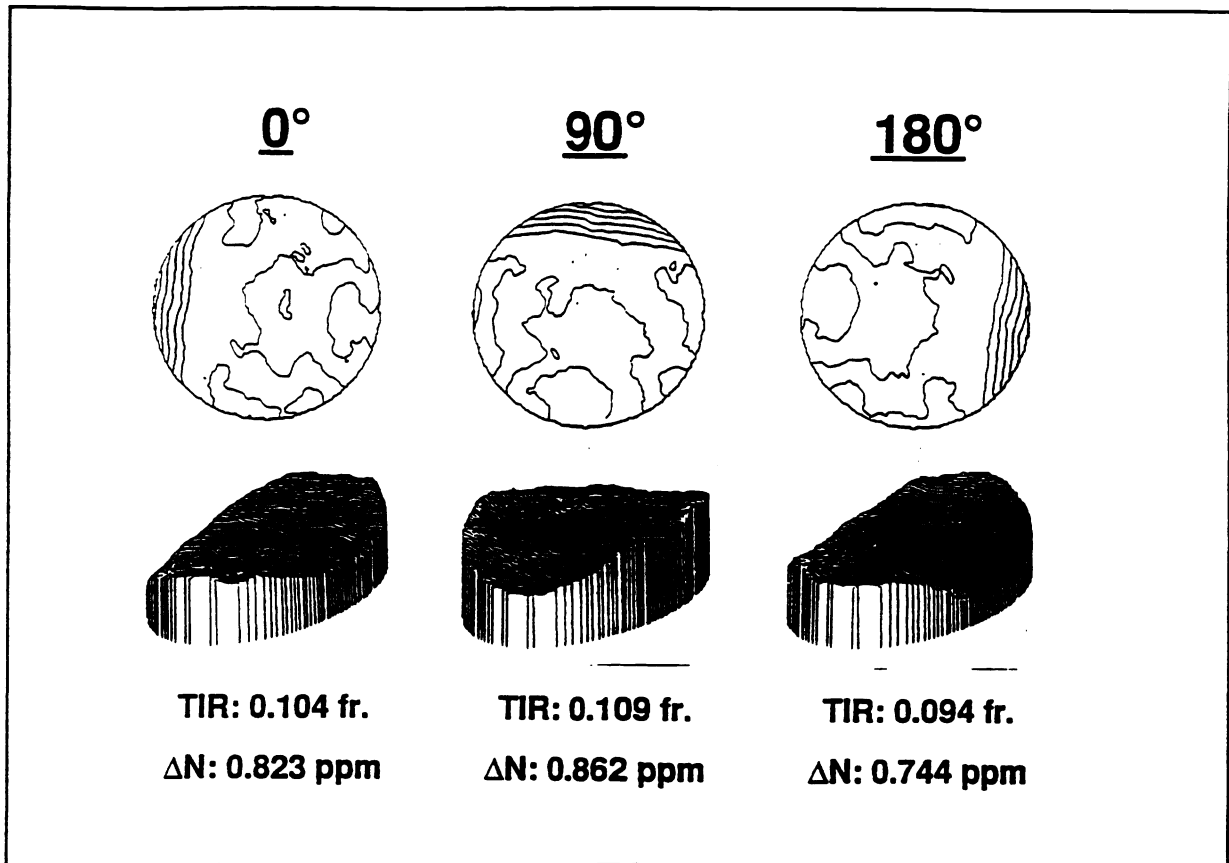


**Figure 3.3** Homogeneity test results [fused silica blank, 40mm thickness, 212mm C.A.].

## 4.2 Description of the Instrument

If a collimated beam of light passes through a prism, it is deviated from its path through some deviation angle. As the prism is rotated, this angle of deviation will reach a minimum when the incidence angle and the exit angle of the prism are equal. Once the angle of minimum deviation and the apex angle of the prism are known, the index is simply computed from the following formula:

$$n = \frac{\sin\left(\frac{A+D}{2}\right)}{\sin\left(\frac{A}{2}\right)} \quad (4.1)$$

where  $A$  is the prism apex angle and  $D$  is the angle of minimum deviation. Taking partial derivatives of the above equation shows that the sensitivity of the index is roughly 3 parts in the sixth place for an error of 1 arc second in these angles. This sensitivity decreases with larger apex angles, but so does the effective aperture of the prism. A prism apex angle of 60 degrees has been chosen as a compromise between radiometry and sensitivity. Tropel's refractometer measures angles, prism apex

and minimum deviation, which defines it as a goniometer. The tremendous improvement of accuracy of the refractometer over a classical visual goniometer is due to the following reasons:

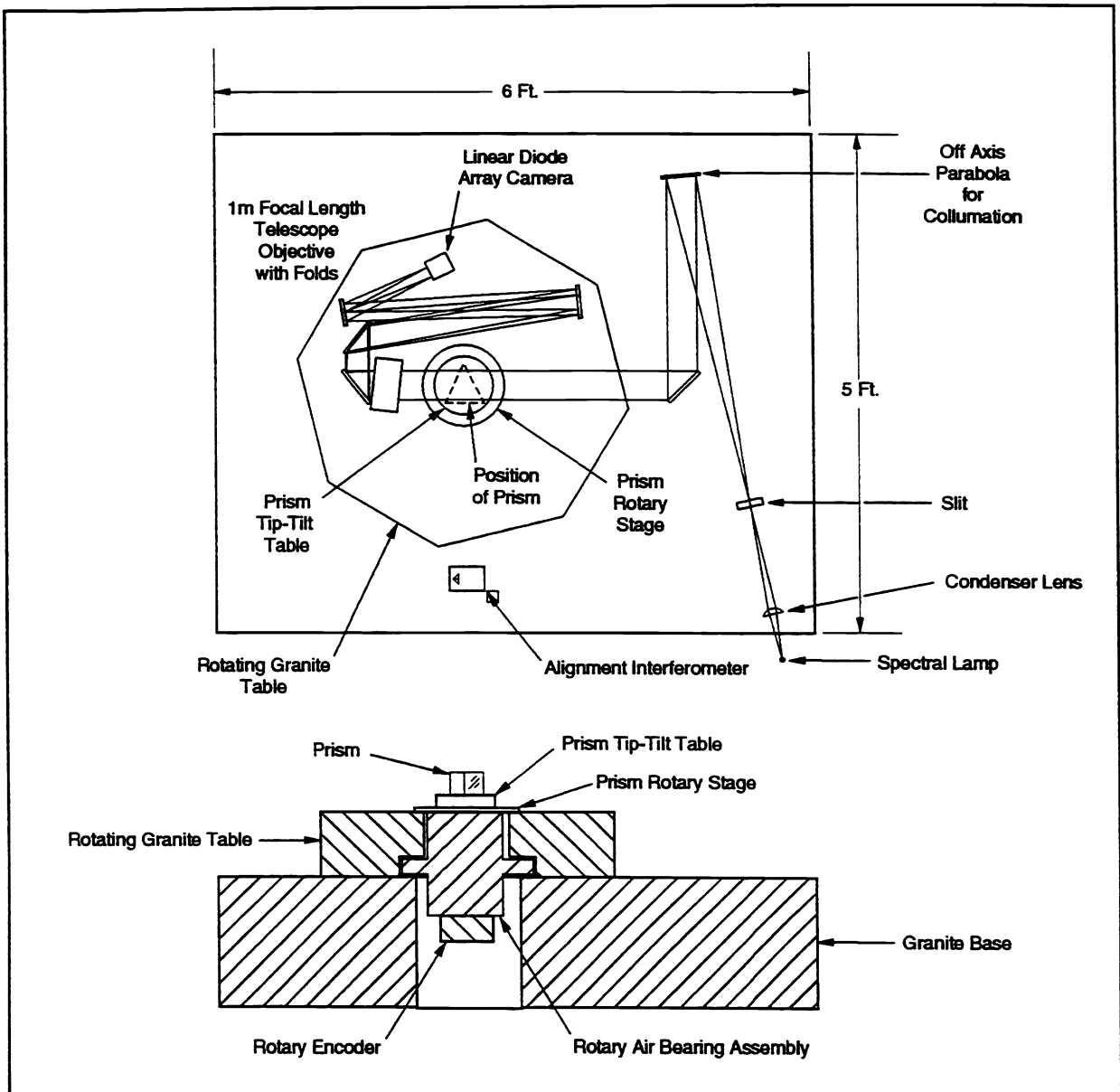


Figure 4.1 Refractometer component diagram.

**4.2.1 Long focal length optics with high resolution linear diode array camera.** The telescope objective translates changes in direction of collimated light in the prism space to changes of position at the camera diode array. The angular resolution of the setup increases with focal length of the telescope. The trade off is that for a certain size prism the  $f/number$  of the imaging also increases with focal length. An increased  $f/number$  means larger line spread due to diffraction and less irradiance at the detector. A study of spectral lines, expected diffraction spread, slit sizes, prism sizes and radiometry of the camera concluded that a 1 meter focal length provided a good balance. The 1" diode array has

2024 pixels, which translates to 2.6 arc seconds per pixel. The slit is the source of the collimator, and the study mentioned also found that a 1 meter focal length collimator was a good compromise between magnification of the slit at the camera array and overall size of the refractometer [Fig. 4.1].

**4.2.2 Mechanical stability.** The size of the optical layout, plus the requirements of stability and rotational integrity made the mechanical design of the refractometer a difficult one. The foundation or base of the refractometer is a 3 ton granite table. The granite is not only rigid and provides a good thermal sink, but also provides a polished flat surface for pneumatically floating a second granite table. The top table, or rotary table, weighs roughly 900 lbs and yet can be floated with several PSI of air and turned with the slightest force. When the air is off, it provides a static base for the telescope objective and camera. A precision air bearing connects the rotary table to the base and maintains the centricity of the table's rotation. A second air bearing is aligned inside the first for maintaining rotational integrity of the prism stage.

**4.2.3 High precision rotary encoder.** The prism rotary stage is coupled to a rotary encoder, which can also be coupled to the granite rotary table by the locking of one of the air bearings. This allows the instrument to track rotation of the prism and telescope objective with measurement steps of 0.035 arc seconds, which exceeds the resolution of the camera.

**4.2.4 Computer control of measurements.** The prism rotary stage is turned by a stepper motor controlled by an IBM PC computer. The computer also records the output from the rotary encoder and camera. Use of the computer allows the acquisition of large sets of data and the use of sophisticated algorithms for the computations of angles from the data.

**4.2.5 Interferometric alignment of the prism.** Each measurement requires the prism faces to be aligned to the stage's rotational axis. A simple visual interferometer was designed for this purpose. The interferometer sits upon a 3" x 4" tip-tilt table and makes use of a corner-cube prism as the reference arm. The tip-tilt table is used in aligning the interferometer to the rotational axis prior to aligning the prism. The prism itself is attached to a tip-tilt table that kinematically rests upon the prism rotary stage. After the prism is aligned to the interferometer, the prism is rotated until each face produces a null fringe pattern. The kinematic mount allows the prism and tip-tilt table to be removed and replaced from the rotary stage without losing alignment. This allows several prisms to be aligned consecutively for measurement after thermal stabilization.

**4.2.6 Environmental isolation, measurement and correction.** The top of the refractometer base is inclosed in a chamber to reduce thermal shifts. After a group of prisms are aligned, they remain inside the chamber for 24 hours, so that they have thermally stabilized before the measurements. The temperature, air pressure and relative humidity are monitored during the measurements. The absolute refractive index of the material is only altered by temperature, but the refractive index of air is influenced by all three.<sup>9</sup> Part of the calculations of the index from the measurements is the conversion of the indices from the environmental conditions of the measurement to a standard condition.

### **4.3 Description of the measurement**

**4.3.1 Angular calibration of the camera.** Prior to measurements of prisms, the camera is angularly calibrated. The calibration provides an equation that describes the angle in the prism space as a function of pixel number. The equation is a polynomial fitted to data points obtained by stepping the granite rotary table through the field of view of the telescope. At each step, an angular position is recorded from the rotary encoder and the spatial position from the energy centroid of the image of the slit is determined.

**4.3.2 Prism apex angle.** The prism's apex angle is measured by light from the collimator reflecting off a face of the prism and through the telescope objective to the camera. The granite rotary table is rotated as close to the collimator as allowed so the illumination of the prism by the collimator will be nearly normal to the prism faces. The first and then the second face of a prism is stepped through the angular field of view of the telescope objective while the computer records the angular position of the prism from the rotary encoder and energy centroid position of the reflected light at the camera. Similar to the angular calibration of the camera, each of the scans are fitted to a polynomial. The average difference between the two polynomials gives the compliment of the apex angle. The distinct advantage of this procedure is that the determination of the centroid of the reflected light is averaged over different positions on the camera array. Likewise, the data from the rotary encoder is averaged over multiple positions.

**4.3.4 Angle of minimum deviation.** The initial direction of the light from the collimator is measured with the prism removed from the rotary stage. The telescope objective is locked to the rotary encoder and the centroid of the un-deviated light is noted. The granite rotary table with the telescope and camera is then floated and rotated to the expected angle of minimum deviation. Once the granite rotary table is positioned, the pixels of the camera can be translated to angles of deviation with the information of the angular calibration of the array, the position on the array of the undeviated centroid and the rotation of the telescope objective. The angle of minimum deviation is determine by stepping the prism through a range of angles and noting the centroid position of each spectral line detected on the camera array. The actual angular position of the prism is not needed for the index measurement, but the computer uses the information for two purposes [Fig. 4.2]. First, the computer steps the prism through four degrees of rotation at the minimum deviation angle collecting data at 20 positions. The second purpose is for fitting the energy centroid position of a spectral line as a function of prism rotation to an equation. The minimum of this equation is translated to angular deviation so as to provide the angle of minimum deviation. The advantage of this technique is that multiple positions of centroids over a range of pixels of the camera are used to determine the position on the diode array of the point of minimum deviation. The parameters of this procedure where partly determined by a Monte Carlo simulation. This Monte Carlo simulation was also useful in providing an error analysis of the refractometer.

**4.3.5 Fitting indices to a dispersion equation.** Measurements for i-line (365 nm) and Krf excimer (248 nm) lenses are performed at several wavelengths since dispersion and index are needed.<sup>10</sup> Dispersion information is more crucial than index because some chromatic corrections are very difficult to impossible to correct after a lens is assembled. In almost all cases, the index data is needed at wavelengths other than what is measured. This requires fitting the index measurements to a dispersion equation that provides index as a function of wavelength. Different forms of equations have been developed through the years, such as Conrady, Herzberger and Sellmeier.<sup>11,12</sup> One that is commonly use is:<sup>6</sup>

$$n^2 = A_0 + A_1\lambda^2 + A_3\lambda^4 + A_4\lambda^6 + A_5\lambda^8 \quad (4.2)$$

This is referred to as the Schott dispersion equation and the A coefficients are provided by glass manufactures for any particular glass type. They are computed from measurements from many melts over the visual region. It can be argued that a Sellmeier equation more accurately describes the physics of the refraction of the material, but the Schott equation has some advantages over a narrow bandwidth.<sup>13</sup> The key to improved dispersion fitting is the fitting of more wavelengths over the region of interest.

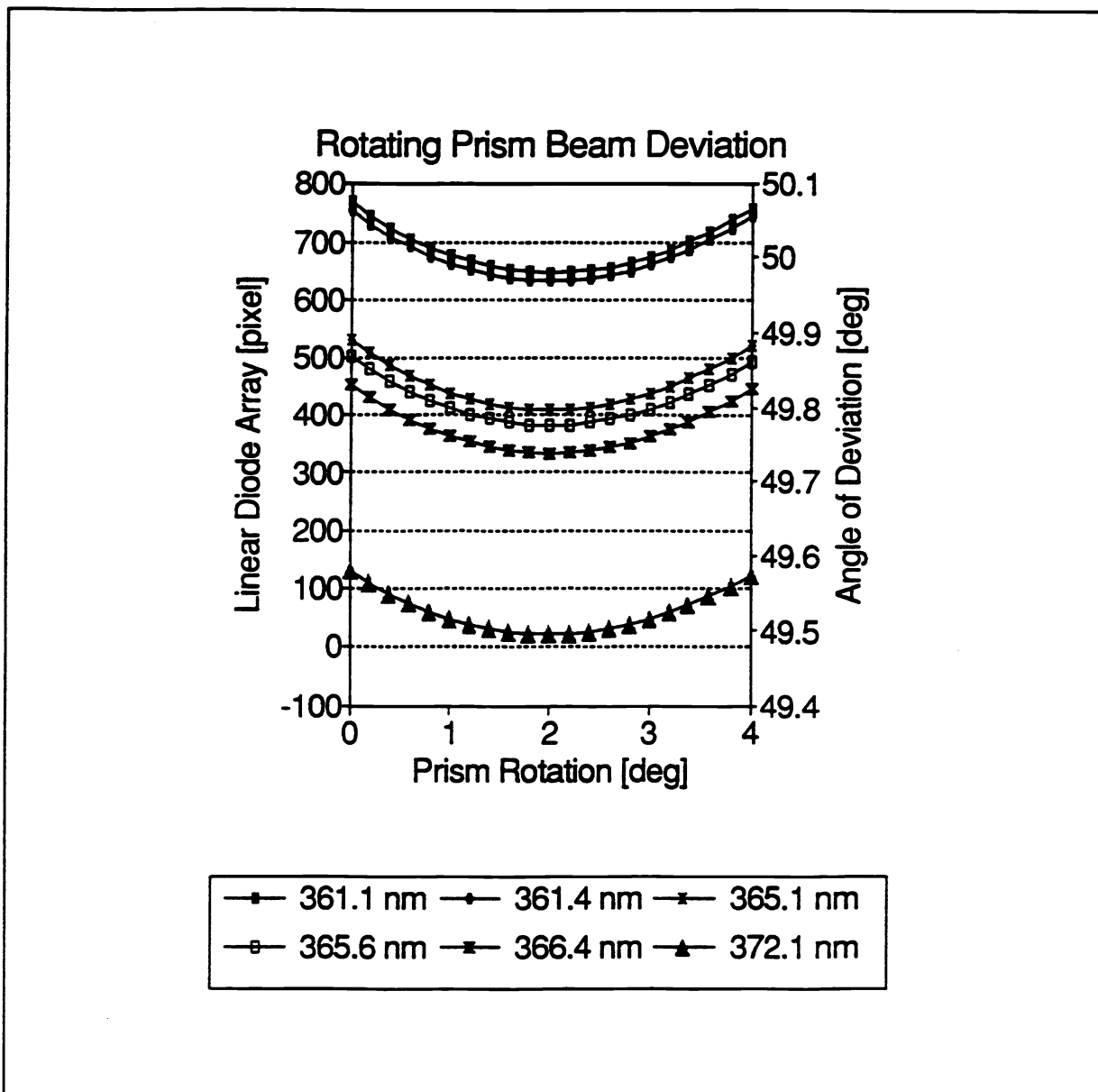


Figure 4.2 Deviation of a beam through a rotating prism.

#### 4.4 Accuracy of the instrument

**4.4.1 Error due to determination of wavelength.** The question of accuracy often leads to the question of wavelength. A 1 Å error of wavelength can produce as much index error as 60 parts in the sixth place. The width of the hyperfine structure of the main Hg i-line can be equated to 3 parts in the sixth place for a flint glass.<sup>14</sup> The wavelength values used are taken from the MIT Wavelength Tables and are set to the centroid position of the spectral line viewed on the diode array.<sup>15</sup> The width of the spectral line is a function of the diffraction and aberrations of imaging the slit through the prism, the width of the slit, the spectral bandwidth of the line and the performance of the diode array. One advantage of this refractometer is that multiple spectral lines can be read simultaneously. This

reduces the source of errors in measuring the dispersion of the sample. The camera diode array can view a spectral span of 35 to 70 nm depending on the dispersion of the material. Once again the accuracy improves with the number of spectral lines measured, due to the averaging of any random error in the determination of the wavelengths. Since we need to measure dispersion more accurately than index, systematic error in wavelength is not as serious.

**4.4.2 Prism apex angle measurements.** A comparison of apex angle measurements on two prisms was performed with NIST. The difference between measurements was found to be 0.3 and 0.9 arc seconds with NIST reporting 3 standard deviations of repeatability at 0.05 arc seconds. A long term study has shown Tropel's 3 standard deviations of reproducibility to be 0.38 arc seconds. As noted previously, 1 arc second of error in apex angle equates to ~3 parts in the sixth place error in index.

**4.4.3 Index measurements.** Our index measurements have proven successful in predicting the achromatization of completed lenses. It also has been one of the components in successfully modelling lenses for adjustments. A long term study at Tropel has shown that the index measurements have a reproducibility of 3 standard deviations of 3.6 parts in the sixth place. A comparison was done with M. Dodge using the same index measurement technique outlined in Malitson's paper<sup>10</sup> at two visible spectral lines. The difference between measurements were found to be 12 and 19 parts in the sixth place. The repeatability of Dodge's measurements was on the order of 3 standard deviations of 9 parts in the sixth. The environmental corrections of these measurements were performed at Tropel. A second comparison was performed with an optical glass manufacturer for five spectral lines around the Hg i-line region for two prisms. The average difference in index between the Tropel measurements and their measurements is 9 parts in the sixth place with a standard deviation of 2 parts. The dispersion over the region was found to be within 1 part in the sixth place.

## 6.0 CONCLUSION

This paper discussed each step in the material qualification of material for microlithographic and other precision lenses. Fluorescence testing determines the absorption characteristics of the material at UV wavelengths. The homogeneity testing determines the variations in the index of refraction of the material to less than 1 E-6 precision and models these variations through the use of Zernike polynomials. Finally, the refractive index testing determines the absolute refractive index and the dispersion of the sample. Thus, the material qualification developed at Tropel provides information for qualifying material to the tight specifications needed.

## ACKNOWLEDGEMENTS

The authors would like to acknowledge F. DeWitt and M. Dunn in their design work on the original Tropel Refractometer. Other contributors to the material qualification program include T. Banister, J. Teleska, S. Mack, J. Platten, J. Webb, and J. H. Bruning.

## 7.0 REFERENCES

1. D. L. Griscom, "Optical properties and structure of defects in silica glass," *J. Cer. Soc. Japan* 99, 923-942 (1991).

2. W. P. Leung, M. Kulkarni, D. Krajnovich, and A. C. Tam, "Effect of intense and prolonged 248 nm pulsed laser irradiation on the properties of ultraviolet-grade fused silica," *Appl. Phys. Lett.* 58, 551-553 (1991).
3. G. C. Escher, "KrF laser induced color centers in commercial fused silicas," *Proc. SPIE* 998, 30-37 (1988).
4. R. A. Weeks and E. Sonder, "The relation between the magnetic susceptibility, electron spin resonance, and the optical absorption of the  $E_1'$  center in fused silica," in *Paramagnetic Resonance 2*, W. Low, ed. (Academic Press, 1963), pp. 869-879.
5. I. Adachi, T. Masuda, and S. Nishiyama, "A testing of optical materials by the Twyman type interferometer," *Atti Fond. Giorgio Ronchi Contrib. 1st. Naz. Ottica* 16, 666-674 (1961).
6. *Optical Glass*, Schott Optical Glass, Inc., Duryea, PA.
7. J. Schwider, R. Burow, K. E. Elssner, R. Spolaczyk, and J. Grzanna, "Homogeneity testing by phase sampling interferometry," *Appl. Opt.* 24 (18), 3059-3061 (1985).
8. C. Ai and J. C. Wyant, "Measurement of the inhomogeneity of a window," *Opt. Eng.*, Vol. 30, No. 9, 1399-1404 (1991).
9. B. Edlen, "The refractive index of air," *Metrologia*, pp. 71-80 (1965).
10. I. H. Malitson, "Interspecimen comparison of the refractive index of fused silica," *J. OSA* 55 (10), 1205-1209 (1965).
11. M. Herzberger, "Color correction in optical systems and a new dispersion formula," *Opt. Acta* 6, 197 (1959).
12. L. E. Sutton and O. N. Stavroudis, "Fitting refractive index data by least squares," *J. OSA* 51 (8), 901-905 (1961).
13. B. Tatian, "Fitting refractive-index data with the Sellmeier dispersion formula," *Appl. Opt.* 23 (24), 4477-4485 (1984).
14. M. H. Keirns and S. D. Colson, "Analysis of the hyperfine structure of the mercury  $6^3D_3$ - $6^3P_2$  transition," *J. OSA* 65 (12), 1413-1417 (1975).
15. *MIT Wavelength Tables, Volume 2, Wavelength by Element*, F. M. Phelps, ed., (MIT Pres, Mass., 1982).